Rendering Depth of Field and Bokeh Using Raytracing

John Andrews Daniel Lubitz

Spring 2019

Abstract

One hallmark of the modern camera is the distinctive, non-smooth blurring of out-of-focus objects, an effect referred to as bokeh, which results from the optical properties of the camera's system of lenses. This effect is often exploited by photographers for artistic effect, but has often been disregarded in graphics due to its complexity and computational cost. Using raytracing and a virtual lens system, we simulate this effect.

1 Introduction

Computer graphics traditionally makes use of a pinhole camera model for rendering scenes. In this model, each point on the image plane is reached by exactly one ray of light from the scene, namely the ray defined by the image plane point and the camera aperture. Consequently, no part of the scene is blurred or out of focus.

Real photography, however, abandoned pinhole cameras long ago. When they are constrained by the laws of physics, pinhole cameras are extremely limiting of the light that reaches the image plane, and therefore require very long exposure times. Real cameras make use of lens systems to allow more light onto the image plane, thus reducing exposure times, while maintaining as much as possible of the tight correspondence between object and image points. They are, however, inherently limited in the range of points for which they can enforce this correspondence. For a given position of the image plane, object points that lie in the corresponding focus plane are projected to a single point, but points not on that plane project onto a circle, called the *circle of confusion,* that grows larger as the object point grows more distant from the focus plane. Points whose circles of confusion are larger than the smallest resolvable disk of the camera sensor or the human eye appear blurred and out of focus; such points are outside of the camera's *depth of field.*

Importantly for our discussion, the circle of confusion is not a smooth blur; it is usually rather sharply defined and more-or-less uniform over its area. "Bokeh" refers to this effect; it is the artistic and aesthetic quality of the out-of-focus parts of an image, in which points of light are blurred into more-or-less clearly defined shapes.

Bokeh is a very desirable effect to mimic in computer graphics; while defocusing might be considered the next best thing for real photography, we are now interested in using it to increase the realism of computer-generated images, and to allow artists another tool to create different aesthetic effects. It is our goal to simulate this effect via raytracing.

2 Related work

In [McGraw, 2015], McGraw simulates defocus blurring by applying synthetic bokeh as a post-processing effect on an otherwise traditionally-rendered image. A pure Gaussian convolution modulated by a depth map is a simple approximation of defocus blurring, though inaccurate; as discussed above, bokeh consists of sharply defined shapes, and a Gaussian blur is too dispersed. A more accurate approximation would be a 2D convolution over the image with a kernel in the shape of the camera aperture; however, full 2D convolutions are computationally expensive. McGraw provides a compromise, using multiple separable, 1D linear kernels on each axis to approximate a sharp 2D convolution kernel, achieving both perceptual accuracy and speed.

In [Wu et al., 2010], the authors instead use a raytracing approach to accurately trace the propagation of light through a camera's lens system. They mathematically model the lens system and refract each ray through each lens surface before emitting it into the scene. This approach has the advantage of realistically capturing bokeh and other lens effects such as spherical aberration, and allows for non-circular aperture shapes and resulting non-circular bokeh, at the cost of performance; a great many samples per pixel are required to integrate the light reaching each image point from the lens with any degree of accuracy. In [Wu et al., 2013], the same team extends this basic approach with even more sophisticated lens effects, including chromatic aberration.

[Joo et al., 2016] go so far as to simulate the lens manufacturing process to create realistic imperfections and artifacts in their bokeh. Additionally, they simulate aspheric lenses. Most lenses are composed of spherical surfaces due to ease of manufacturing, but such lenses suffer from imperfect convergence of transmitted rays (the above-mentioned spherical aberration). Aspheric lenses can produce better focus, but are more difficult to model and manufacture. Joo et al. raytrace such lenses using root-finding methods to produce a very highly-detailed image of the lens system. However, they do not fully raytrace the scene; instead, they use the raytraced lens system image to modulate a traditional rendering, in a manner similar to a 2D convolution.

Our approach is most similar to that of [Wu et al., 2010].

3 Overview of Gaussian optics

One of the chief problems of raytracing a lens system is that not all rays cast towards the first lens surface will actually make it through the system as a whole. In fact, for any given point on the image plane, only rays from a relatively small portion of the lens will reach it; the others will be either internally reflected by some lens element, or fail to clear some internal aperture of the system. Uniformly sampling the entire lens surface is therefore very wasteful of resources, and to make the computation reasonably fast, we require some way to narrow down the sample space. Gaussian optics provides us with exactly this, in the form of an exit pupil. To that end, we present here an overview of the relevant concepts from optics. Much of this material is adapted from [Greivenkamp, 2004].

In an optical system, the *aperture stop* is the element that most restricts the light than can enter the image space of the system. It is frequently the physically narrowest element, but not always. Any light that clears the aperture stop will make it to the image plane. The *exit pupil* is the image of the aperture stop in image space; in effect, any light that reaches the image plane will come from the direction of a point in the exit pupil (Figure 1). Hence, the exit pupil defines the sample space for our raytracing. Finding the exit pupil requires building up some background machinery.

To a first approximation, the properties of an optical system can be determined using Gaussian optics. This system assumes all surfaces within the system are ideal refracting or reflecting elements, and makes use of the following small-angle approximations for the sine, cosine, and tangent functions:

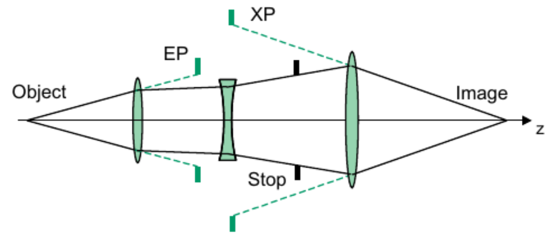

Figure 1: The entrance pupil (EP) and exit pupil (XP). The entrance pupil is the image of the aperture stop in object space; this would be important were we tracing rays from object space into the camera, but for our purposes, we only need the exit pupil. Figure from [Greivenkamp, 2004].

$$\sin x \approx \tan x \approx x$$
$$\cos x \approx 1$$

These are the first-order Taylor expansions of these functions around 0, accurate when $|x|$ is small, and are of great usefulness here due to their linearity.

Gaussian optics considers only systems of spherical elements, axially aligned and rotationally symmetric about that axis. By convention, the optical axis of the system is assumed to be the z axis, with object space towards negative z and image space towards positive z. Each surface is modeled as a single plane perpendicular to the optical axis at the surface's *vertex*, the point at which it intersects the axis. The radius of curvature of the surface is a signed quantity indicating the concavity of the surface; specifically, it is the directed distance from the surface vertex to its center of curvature. Hence, a negative radius of curvature indicates that the surface is concave towards object space, and a positive radius of curvature indicates that it is convex towards the same.

The basic technique of Gaussian optics is to reduce systems of many surfaces to a single set of points on the optical axis, the *cardinal points,* (and their corresponding planes perpendicular to the axis): the front and rear *focal points,* and the front and rear *principal points.* Once these are known, the image of any object point can be found via similar triangle analysis using the following principle: any ray through the front focal point that intersects the front principal plane at a height h from the optical axis emerges from the rear principal plane at the same height parallel to the axis, and vice versa (Figure 2).

For a single surface, the principal planes are coincident at the surface's vertex. The focal points are

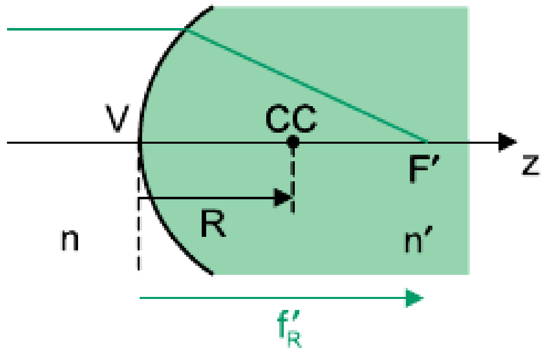

Figure 2: The rear cardinal points of a single surface. The principal points are coincident with the surface vertex V. As demonstrated by the red ray, any object-space ray incident on the front principal plane is transmitted as a ray through the rear focal point F'; a similar rule holds for image space rays and the front focal point F. CC is the center of curvature. Figure from [Greivenkamp, 2004].

found as follows:

$$\text{Optical power } \Phi = \frac{n' - n}{R}$$
$$\text{Effective focal length } f_E = \frac{1}{\Phi}$$
$$\text{Front focal distance } f_F = -n f_E$$
$$\text{Rear focal distance } f'_R = n' f_E$$

where n and n' are the indices of refraction on, respectively, the object space side and the image space side of the surface, and R is the radius of curvature. The focal distances are the signed distances from the surface vertex to the corresponding focal points (Figure 2).

For two elements enclosing a material with index of refraction n_2, with indices $n = n_1$ on the object space side and $n' = n_3$ on the image space side of the pair, we can find their joint principal planes via the following:

$$\tau = \frac{t}{n_2}$$
$$\Phi = \Phi_1 + \Phi_2 - \Phi_1 \Phi_2 \tau$$
$$\frac{d}{n} = \frac{\Phi_2}{\Phi} \tau$$
$$\frac{d'}{n'} = -\frac{\Phi_1}{\Phi} \tau$$

In the above, t is the signed distance from the first element's rear principal plane to the second element's front principal plane; Φ_1 and Φ_2 are the optical powers of the first and second elements respectively, and Φ is the joint optical power; d is the signed distance from the first element's front principal plane to the joint front principal plane; and d' is the signed distance from the second element's rear principal plane to the joint rear principal plane (Figure 3). The joint focal points can be found as above for a single surface, with the exception that f_F and f'_R are now signed distances from the front and rear principal planes respectively, rather than from a surface vertex. Systems of more than two elements can be reduced by repeatedly applying this procedure to adjacent pairs of elements.

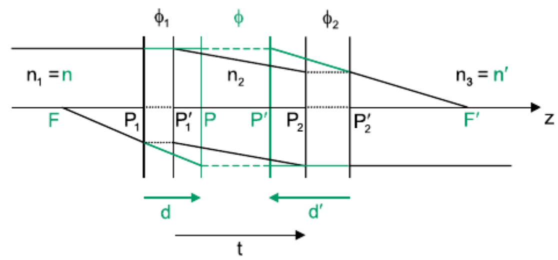

Figure 3: Gaussian reduction of a two-element system. Figure from [Greivenkamp, 2004].

To determine which lens element acts as the system aperture stop, we perform a *paraxial raytrace* through the system. This is a trace of a ray very near the optical axis, which remains near the optical axis throughout the system, and makes use of the small-angle approximations described earlier. The procedure involves alternating two equations: the transfer equation to determine the new height of the ray as it arrives at the next element's front principal plane, and the refraction equation to determine the new angle of the ray as it exits the element's rear principal plane:

$$\text{Refraction: } n'u' = nu - y\Phi$$
$$\text{Transfer: } y' = y + u't'$$

In the above, u is the angle of the ray incident on an element's front principal plane, and u' is the angle of the ray exiting the element's rear principal plane; n and n' are the object and image space indices of refraction around the element; y is the (signed) height above the optical axis of the ray's intersection with the element's principal planes, and y' is the height of the intersection with the next element's principal planes; t' is the signed distance from the element's rear principal plane to the next element's front principal plane; and Φ is the element's optical power (Figure 4).

The refraction equation is based on Snell's law of refraction, using the small-angle approximation. The

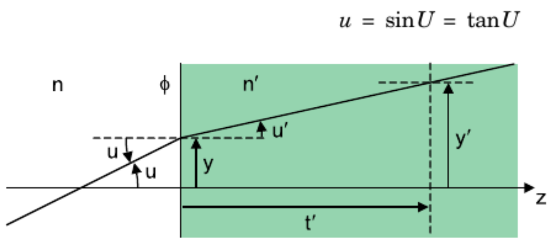

Figure 4: Paraxial raytracing. Figure from [Greivenkamp, 2004].

full law is this:

$$n \sin\theta = n' \sin\theta'$$

The $-y\Phi$ term in the paraxial refraction equation accounts for the changing surface normal as distance from the axis increases.

During a paraxial raytrace, we can record the ratio $|y|/a$ for each element of the system, where a is the aperture radius of that element. The element for which this ratio is greatest — the element for which the ray passes proportionally closest to the aperture — is the system aperture stop. Once we know which element is the system aperture stop, we can reduce the portion of the system behind that element and perform similar triangle analysis to find its image in the image space of the system; that image, finally, is the exit pupil.

This procedure consists of a great many steps, but each one individually is very simple. Computationally, this calculation is among the least expensive parts of our algorithm.

4 Modeling the lens system

Our model considers only spherical optical surfaces. We specify the lens system in its own coordinate space in units of millimeters, axially aligned on the z axis with object space towards negative z, the convention of Gaussian optics. Surfaces are listed from object space to image space, with each surface specified by its radius of curvature, the diameter of its aperture, the index of refraction of the material on the image space side of the surface, and the distance to the next surface's vertex. A surface with a radius of 0.00 is assumed to be planar, and the medium in front of the system is assumed to be air, with index of refraction 1.00. A diaphragm in the system is modeled as a planar surface with air on either side of it. Figure 5 shows one lens configuration using this representation. It should be noted that this is the same representation used by [Wu et al., 2010], and we used the lens system configurations presented in that paper for our examples.

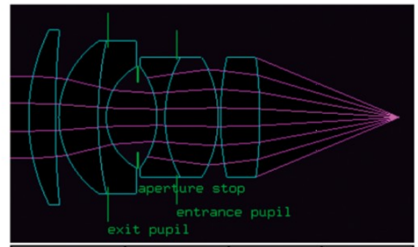

radius	thickness	index	aperture
85.500	11.600	1.744	76.0
408.330	1.500	1.000	76.0
40.350	17.000	1.620	66.0
156.050	3.500	1.621	66.0
25.050	13.700	1.000	44.0
0.000	8.300	1.000	42.6
-36.800	3.500	1.689	44.0
55.000	23.000	1.744	52.0
-51.500	1.000	1.000	52.0
123.500	17.000	1.744	52.0
-204.960	0.000	1.000	52.0

Figure 5: The particular measurement for the lens assembly used for our renderings. Figure from [Wu et al., 2010].

After loading the lens system measurements, our implementation performs a paraxial raytrace, as described above, to determine which element of the system acts as the system aperture stop. We then perform a Gaussian reduction on the portion of the system behind the aperture stop, closer to image space, and use that reduction to find the location and radius of the exit pupil, and this concludes our preprocessing of the lens system.

During raytracing, the lens system can be queried for a ray through any point in the image. To generate a ray, we select a uniformly random point in the exit pupil and create a ray from the queried image point through the pupil point, which we then trace through the lens system.

Due to the way we model the lens system, there is no need to test the ray for intersection with every surface for every step of the lens system trace, or to add an epsilon to intersection points to overcome floating-point error; we know exactly the order in which each ray will intersect the surfaces, and we simply ignore all others for each step. So, in optical order, we intersect the ray with the sphere (or plane) of the next lens surface and determine the surface normal at the intersection point. We use Snell's law to compute the refraction direction, and use this to create a new ray for the next step of the trace.

While the calculation of the exit pupil provides very useful boundaries on our sample space, it is calculated via Gaussian optics, which is an approximation; sampling the exit pupil greatly increases the probability that any given ray will make it through the lens system, but does not provide a guarantee. Therefore, at each surface, we compare the intersection point's distance from the z axis with the aperture radius of that surface, and discard the ray if it exceeds that radius.

After the last surface has been intersected, we transform the final ray into scene space using the inverse of the camera view matrix. From there, the color corresponding to this ray is determined via traditional recursive raytracing. For a single pixel, we cast many rays through the lens, and determine the final color by simple average of the colors returned by those rays.

5 Other implementation details

Our implementation makes use of KD-trees to accelerate raytracing on triangle meshes. After loading the geometry data for each mesh, we compute the centroids of each triangle, and sort them along each axis. Using this, we construct the KD-tree for the mesh by recursively subdividing the mesh's bounding box at the median along the axis with the greatest range of centroids. Triangles that span the divide are included in both subtrees. When testing a ray for intersection with a mesh, we first recursively test for intersection with the KD-tree bounding boxes to generate a list of potentially intersected faces.

We also implemented vertex normal interpolation on the CPU for triangular faces, to allow triangle meshes to appear smooth in our raytraced images. Once an intersection point has been determined on a triangle, we can compute the barycentric coordinates α, β, γ of that point using Cramer's rule. Then, we compute the internal surface normal $\tilde{n}$ as follows:

$$n = \alpha\tilde{n}_a + \beta\tilde{n}_b + \gamma\tilde{n}_c$$
$$\tilde{n} = \frac{n}{\|n\|}$$

where $\tilde{n}_a, \tilde{n}_b, \tilde{n}_c$ are the unit vertex normals of the vertices corresponding to α, β, and γ respectively.

Our implementation utilizes multithreading to accelerate overall rendering times. Upon starting a rendering, we divide the image into a grid of (approximately) 20×20 pixel patches and spawn as many threads as the system has physical processors. Each thread renders a single patch at a time, querying the main image structure for the next unassigned patch after finishing each patch. Raytracing is an inherently parallel algorithm; each pixel in the image can be computed independently of any other pixel. Hence, we see significant speedup using this scheme.

6 Early results and challenges

We began development by implementing a single thin lens and placing it in the world. This proof of concept allowed us to ensure that we could produce a coherent image from a simple system. One feature of this early test platform was that we could trace rays from a point on the image plane to the entire surface of the lens, then visualize those rays. This enabled us to see whether or not the lens was refracting the rays correctly.

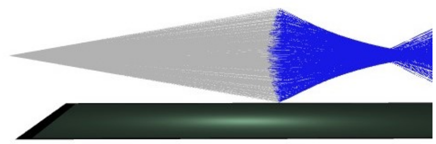

Figure 6: Visualization of one pixel sampling the entire lens surface in the test environment. Because of the spherical lens, the rays do not converge to a single point.

We were able to faintly capture the circle of confusion, meaning our approach was working. The trouble was getting an image that was meaningful, as we were not using proper measurements at this point and the positioning and size of the image plane, lens, and object were essential guesswork.

Figure 7: The circle of confusion created by a small sphere in front of a single thin lens.

The implementation of the thin lens was different from the final project due to this lens being an actual object the exists in the scene. It was made using two intersecting spheres of the same diameter. A hit from a ray on one sphere was checked to make sure it was inside the other in order to be considered on the lens surface.

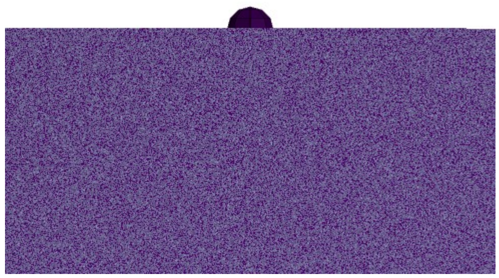

Figure 8: A half-raytraced image of a sphere in front of a thin lens. Due to lack of measurements, the sphere was not the correct size nor in the correct position to get an image from. Some rays missed the sphere and some hit it, creating the static pattern seen here. This is also an example of what may happen with a low smaple count.

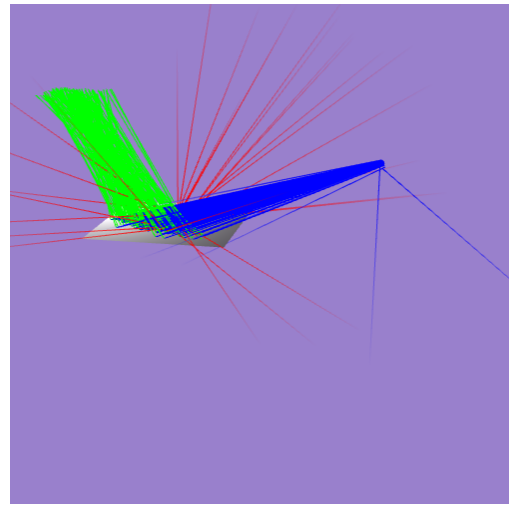

Figure 9: An early bug from our lens assembly implementation. Here we see the effects of a single sign error in our refraction logic, which prevented the emerging rays from converging and caused an occasional ray to actually be emitted backwards from the camera.

The transition to raytracing the full lens assembly was where the most bugs arose, particularly sign errors and vector math. In order to send a ray fully through the assembly, we needed a system that would perform refraction from an arbitrary material into an arbitrary material at a point where the normal may be facing forwards or backwards. It also needed to check for conditions such as collision with one of the stops or a ray refracting at such a steep angle that it would not collide with the next lens. This complexity required many attempts in order to nail down the math.

The nature of raytracing is heavy computation. Because of the way our system gathers light for each pixel from all possible directions out of the lens, we need a large number of samples to generate a realistic image. This hurt testing as we were unable to quickly check if a change to an algorithm actually fixed anything. Adding multithreading dramatically increased our ability to produce images and test at an acceptable rate.

7 Results and discussion

All of the results we present here were rendered on a Lenovo Thinkpad T450s laptop with an Intel i7 4-core processor. We are able to produce accurate images that exhibit the desired depth of field and bokeh effects at 200×200 pixels, with 250 lens samples per pixel, in under ten minutes.

All of our results used the lens assembly pictured in Figure 5, which has an approximate effective focal length of 100 mm. Different depths of field and bokeh qualities may be achieved by different lens configurations; this is one possible avenue for future work.

8 Future work

All lenses and other elements in the lens assembly are perfectly spherical or circular. One possible avenue for further study would be to implement the option to change these parameters and introduce aspheric lenses to the system. Additionally, rendering an image using a non-circular aperture stop would yield particularly interesting results, given that the circle of confusion's shape on the image plane is dictated by the shape of the aperture stop. This would involve more sophisticated raytracing algorithms as the intersection detections would no longer be simple equations. Actual modeling of the lens surfaces could be done, but that would increase computation time significantly. Pupil calculation would also need to be reworked if the aperture could change shape.

In our system, we model light as a single color: white. In reality, light is not a simple white but is instead made up of different wavelengths. In order to accurately model lens interactions with varying wavelengths of light, a more complete version of Snell's law would need to be put in place. In addition, finding a

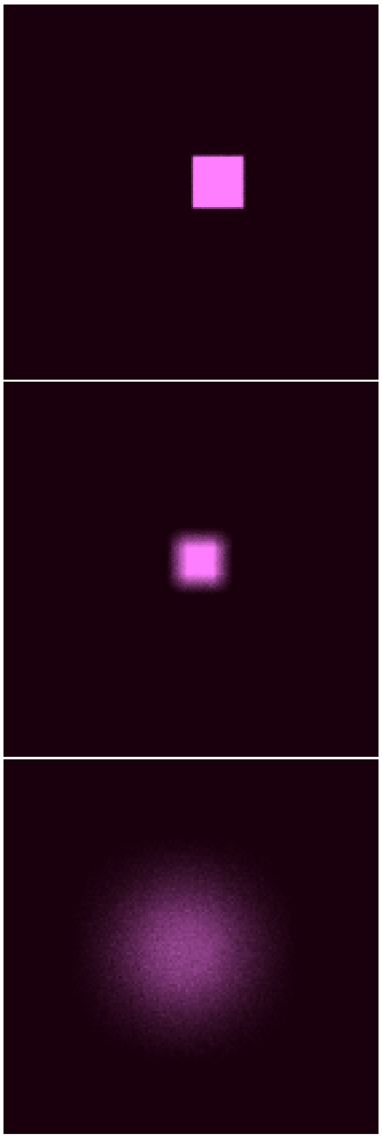

Figure 10: A progression of images of a single square light source as the camera zooms further out and the light becomes more out of focus. Note that the defocus blur is remarkably smooth; this may be a result of the specific lens configuration used. Other combinations of focal lengths and aperture diameters will produce different bokeh qualities.

Figure 11: High resolution render of reflective bunnies. Depth of field is clearly apparent with the ground plane. 500×500 pixels, 500 lens samples per pixel, approximately 2.5 hours.

way to make raytracing with multiple rays each with individual wavelengths efficient is non-trivial. Having more than one color of ray to cast means many times more rays in total to compute. Adding this would allow the system to create chromatic aberration artifacts, adding to the realism of the image.

Taking the idea of replicating camera effects further, another feature to implement could be lens flare. This results from scattering in the lens assembly, usually caused by imperfections in the material makeup of the lens elements. Another artifact not modelled is refection of light off of the lenses. We only perform complete refraction but some of the light is reflected internally.

Because our system is modular in the sense that the lens assembly is specified through a file separate from the rest of the scene, it would be possible to experiment with various types of configurations, including setups that feature mirrors. In this way, perhaps certain reflecting telescopes and microscopes could even be modeled.

The major performance bottleneck of our system is not the lens assembly itself, but rather the recursive raytracing that takes place in the scene. This is especially expensive when rendering high-complexity meshes like the Stanford Bunny. Nonetheless, since each trace of the lens assembly is essentially the same, it would be possible, and possibly beneficial, to calculate the lens samples offline and store them as part

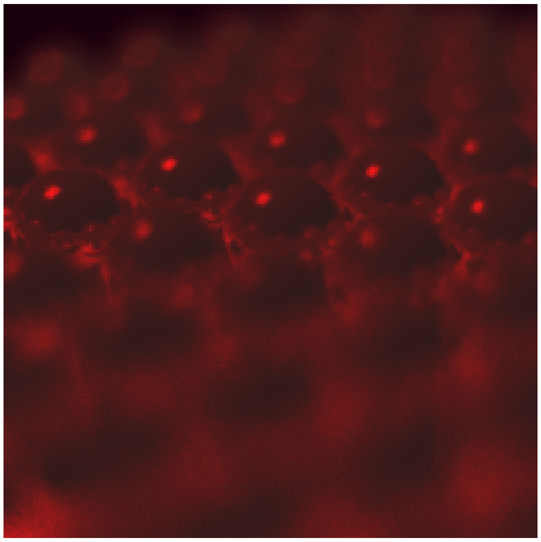

Figure 12: An array of red reflective spheres under a red light, with noticeable bokeh in the out-of-focus specular highlights. 200×200 pixels, 250 lens samples per pixel, roughly 8:15 minutes.

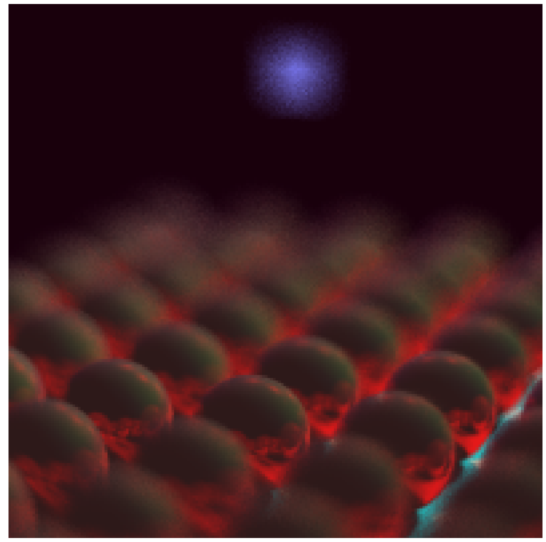

Figure 13: Array of red reflective spheres with blue light patch showing circular bokeh effect. The blurring on the light is significantly smoother than we would like; c.f. the discussion under Figure 10. 200×200 pixels, 250 lens samples per pixel, approximately 9 minutes.

of the lens configuration. This would require a large amount of storage; each pixel in the image has a different set of samples. It is unclear if this would result in a speed increase during the actual rendering, and this might be an interesting experiment.

A possible enhancement to the efficiency of the raytracer would be to use a dynamic sampling technique. Because we are required to use many a large number of rays for each pixel, being able to cut down on that requirement would mean great time savings. For this technique, we would only send out for pixels where there is a large variation in returned color. The greater the variation, the more samples would be necessary to capture the true result. For pixels where most of the rays come back looking the same, not many more rays would need to be used to approximate the true color.

9 Attributions

John Andrews Wrote the raytracing engine, KD-tree implementation, and vertex normal interpolation. Wrote parsers for scene and materials files. Did the optics math for finding the exit pupil. Integrated the lens and lens assembly data structures with the rest of the raytracer. Rendered most of the examples.

Daniel Lubitz Created early test environment to ensure viability of strategies, worked out initial lens refraction math, implemented early version of raytracing system for lenses, developed lens and lens assembly data structures and file conventions, Windows compatibility debugging.

References

[Greivenkamp, 2004] Greivenkamp, J. E. (2004). *Field Guide to Geometrical Optics*. SPIE Field Guides. SPIE Press.

[Joo et al., 2016] Joo, H., Kwon, S., Lee, S., Eisemann, E., and Lee, S. (2016). Efficient ray tracing through aspheric lenses and imperfect bokeh synthesis. *Computer Graphics Forum*, 35(4):99–105.

[McGraw, 2015] McGraw, T. (2015). Fast bokeh effects using low-rank linear filters. *The Visual Computer*, 31(5):601–611.

[Wu et al., 2010] Wu, J., Zheng, C., Hu, X., Wang, Y., and Zhang, L. (2010). Realistic rendering of bokeh effect based on optical aberrations. *The Visual Computer*, 26(6):555–563.

[Wu et al., 2013] Wu, J., Zheng, C., Hu, X., and Xu, F. (2013). Rendering realistic spectral bokeh due to lens stops and aberrations. *The Visual Computer*, 29(1):41–52.